Supplementary Information to

Group 10 Metal-Thiocatecholate-Capped Magnesium Phthalocyanines – Coupling Chromophore and Electron Donor/Acceptor Entities and its Impact on Sulfur Induced Red-Shifts

Authors

Malcolm Alan Bartlett and Jörg Sundermeyer

Contents **Page**

FTIR Spectra

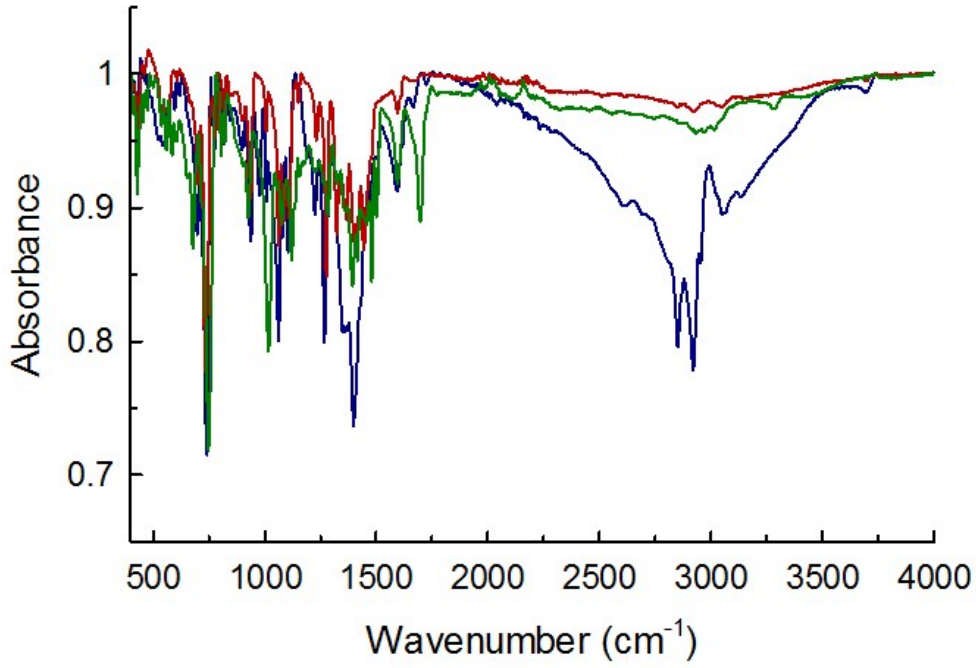

Figure S1. Overlay of FTIR spectra for [$(RS)_8$PcMg] (blue), [$(^{Me}RS)_8$PcMg] (red) and [$(^{Me2}RS)_8$PcMg] (green).

UV-Vis spectra for molar absorbance coefficient determination

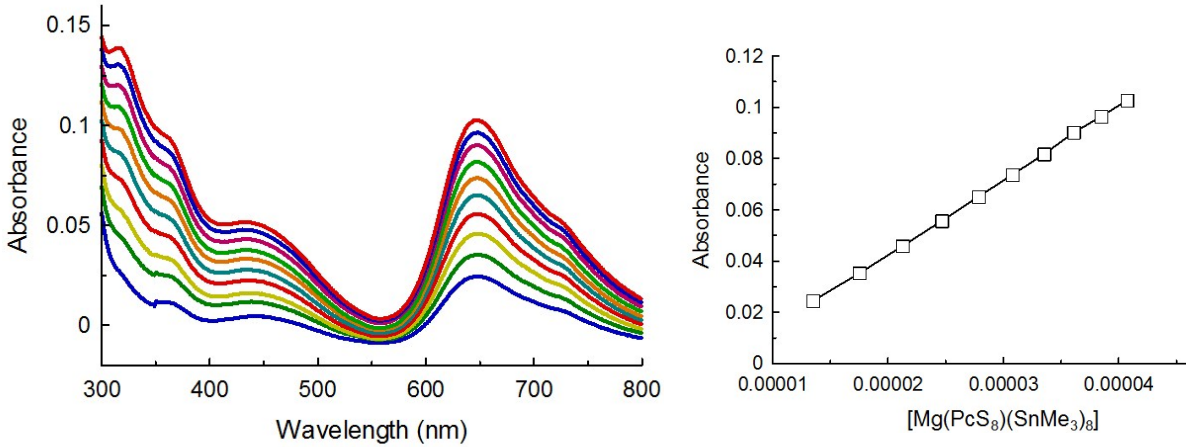

Figure S2. (Left) Absorption spectra for $[(Me_3Sn)_8(S_8PcMg)]$ at different concentrations. (Right) Plot of absorbance at 648 nm vs. concentration to determine the molar attenuation coefficient for the complex. The linear response shows the spectra are for a monomeric species rather than a dimer or other aggregate.

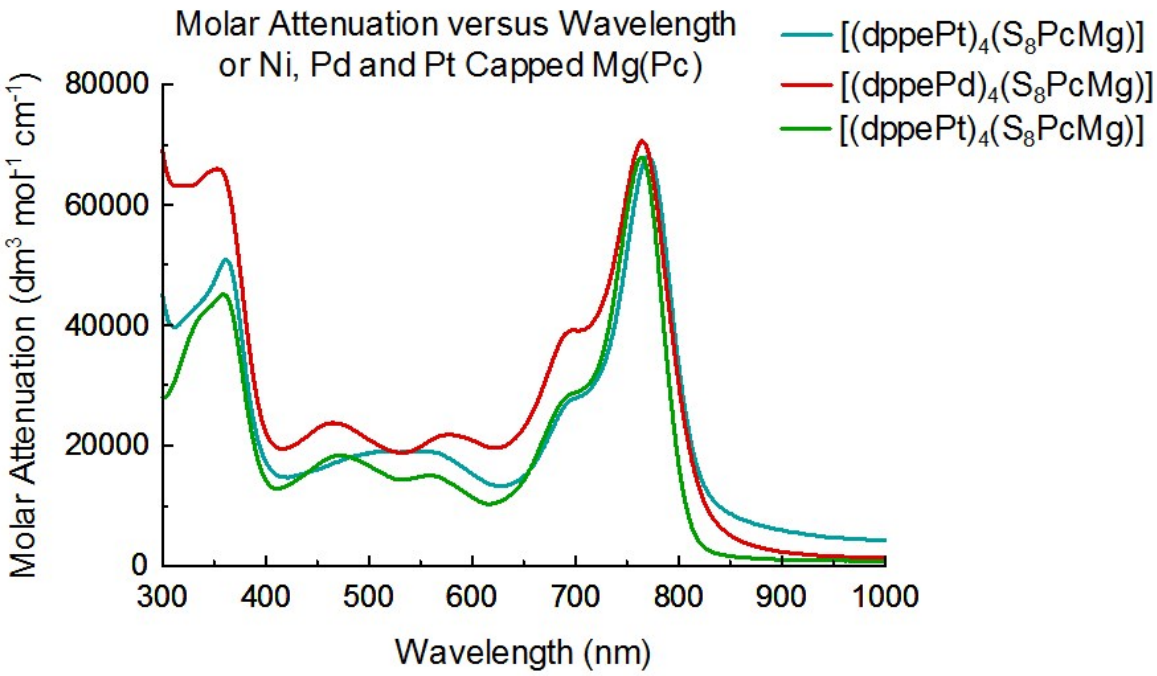

Figure S3. Molar attenuation for the group 8 metal-capped Mg(Pcot) complexes.

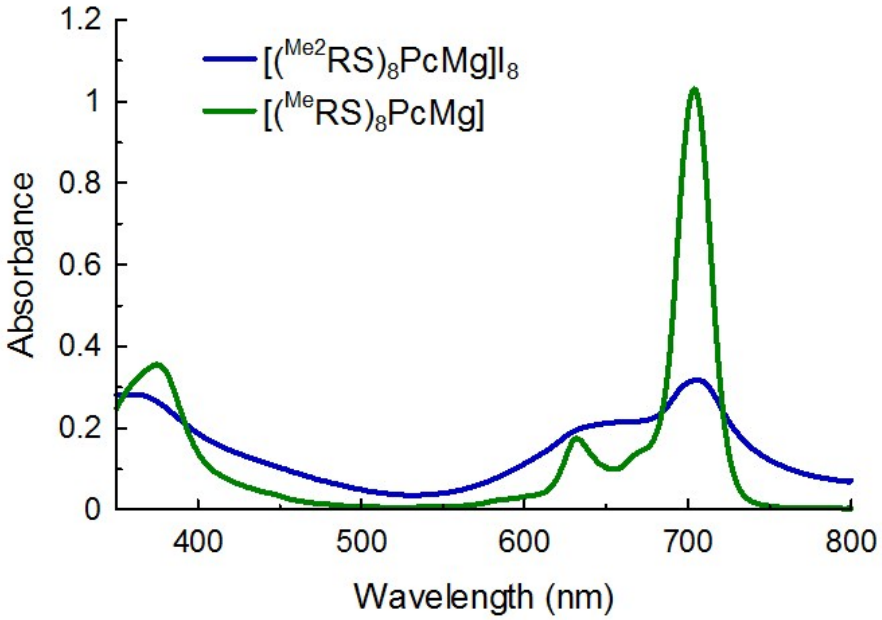

Figure S4. UV-Vis absorption spectra for [(^{Me}RS)$_8$PcMg] (green) and [(^{Me2}RS)$_8$PcMg] (blue) in DMF. As can be seen, aggregation is promoted by quaternerisation of the Pc ligand.

TDDFT Results

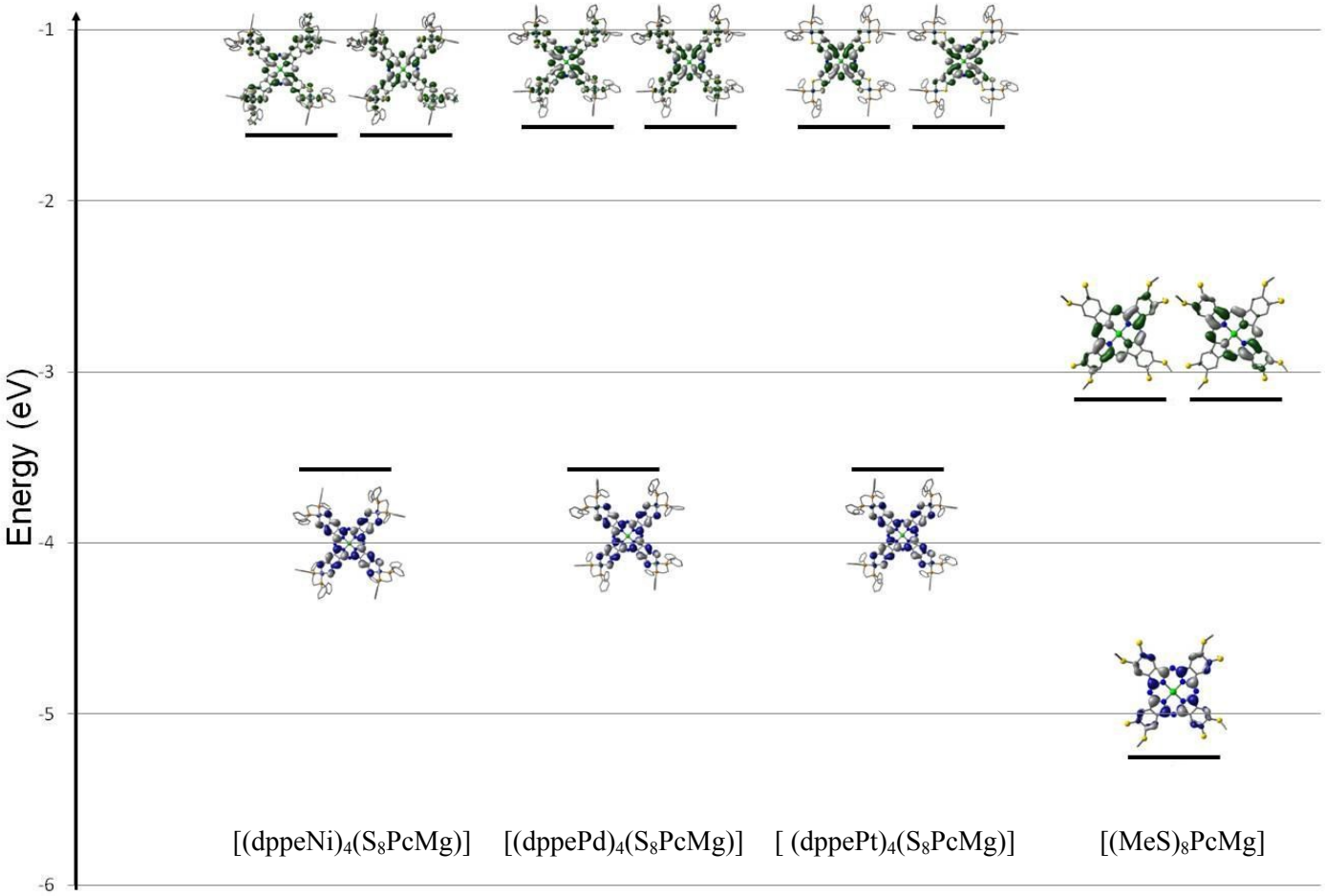

Figure S5. MO energy level diagram of the HOMO, LUMO and LUMO+1 for $[(dppeNi)_4(S_8PcMg)]$, $[(dppePd)_4(S_8PcMg)]$, $[(dppePt)_4(S_8PcMg)]$ and $[(MeS)_8PcMg]$. Occupied orbitals are coloured blue and grey, and unoccupied orbitals are coloured green and grey.

Copies of NMR spectra of studied Pcs

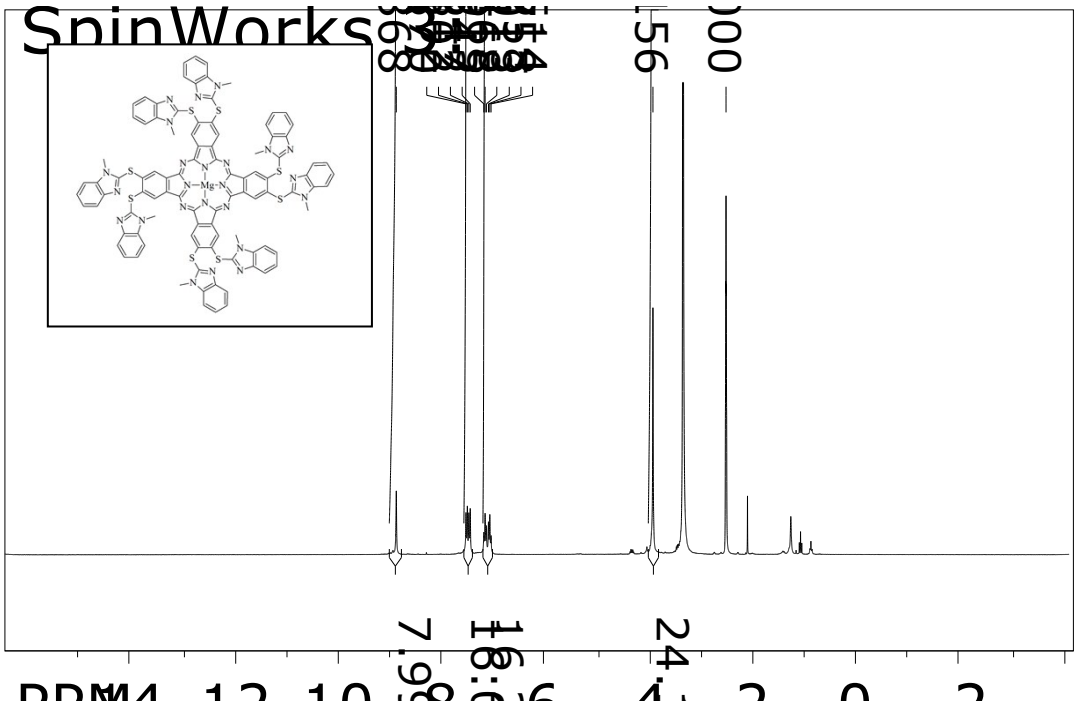

Figure S6. ^{1}H NMR of [(^{Me}RS)$_8$PcMg] in DMSO-*d6*

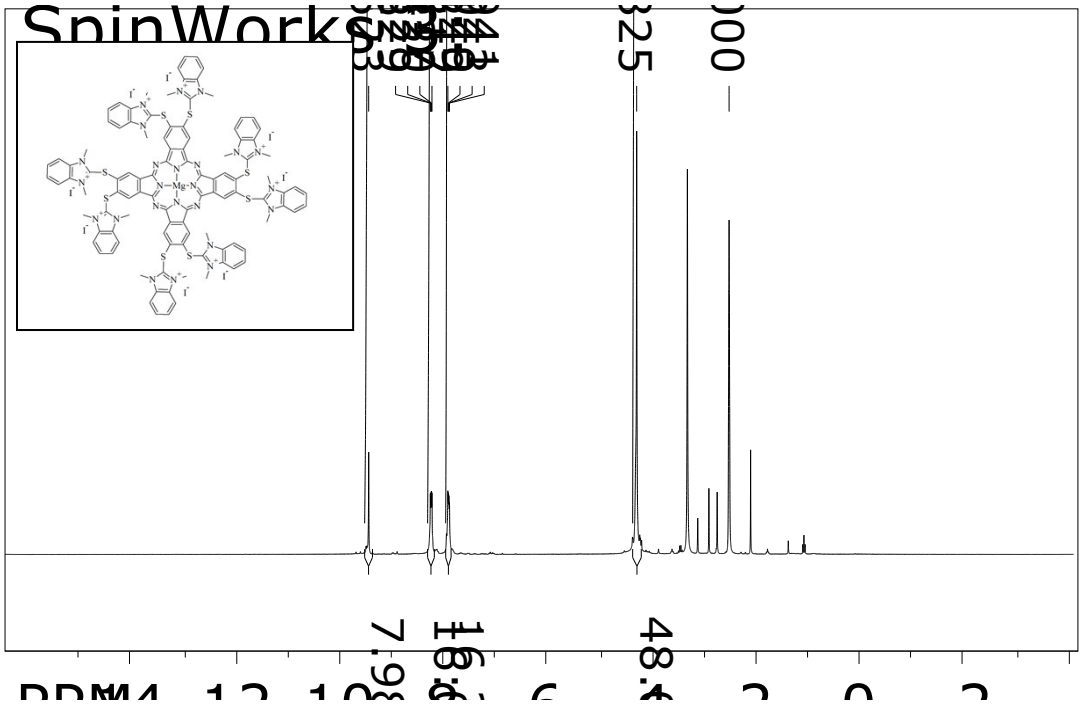

Figure S7. ^{1}H NMR of [(^{Me2}RS)$_8$PcMg] in DMSO-*d6*

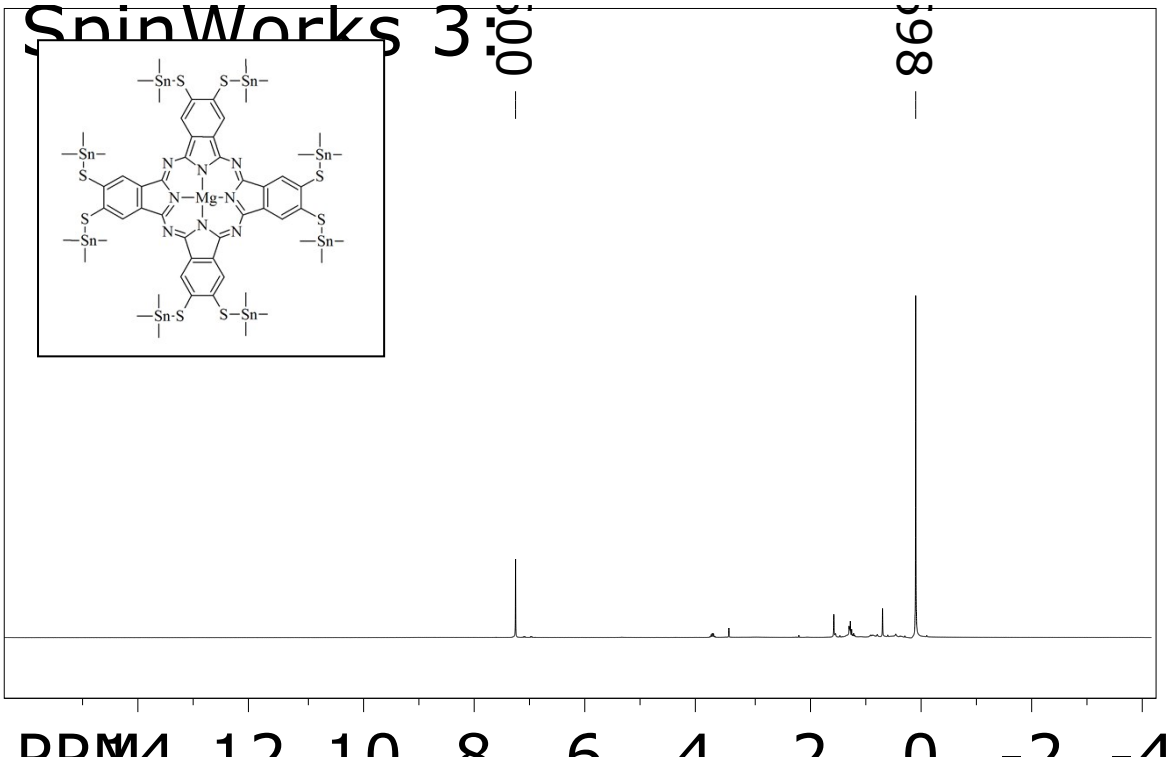

Figure S8. ^{1}H NMR of $[(Me_3Sn)_8(S_8PcMg)]$ in $CDCl_3$

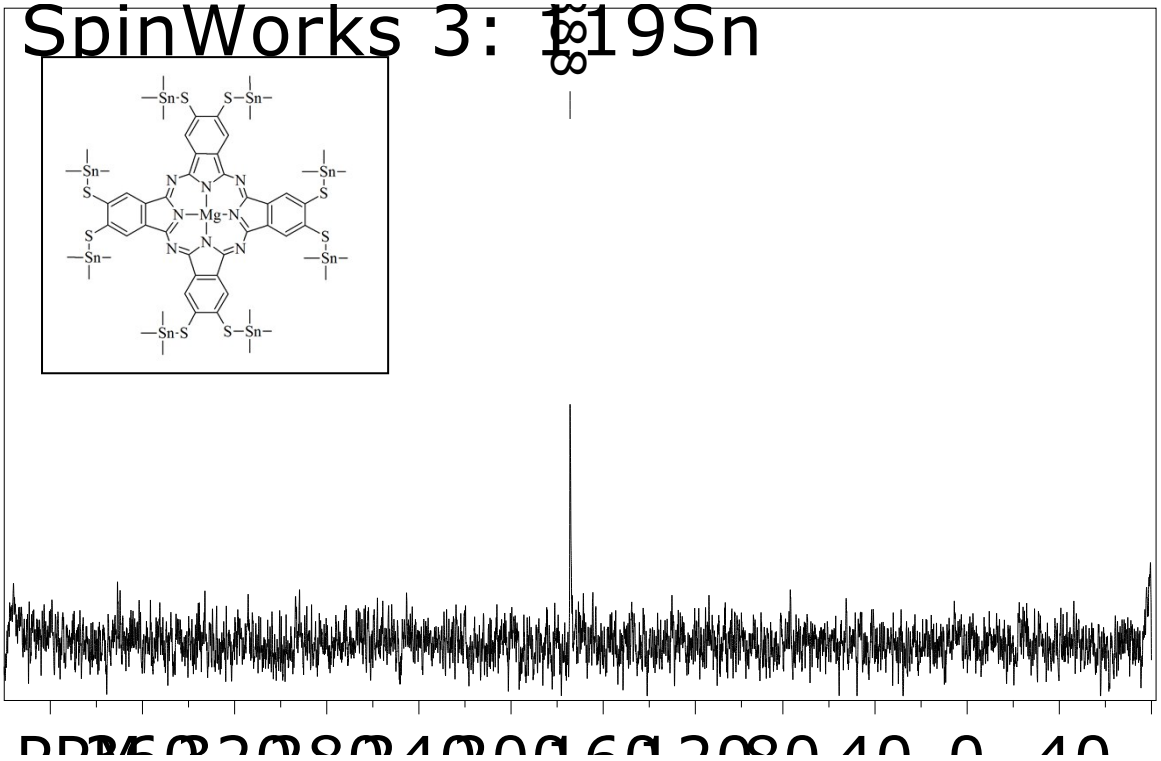

Figure S9. ^{119}Sn NMR of $[(Me_3Sn)_8(S_8PcMg)]$ in $CDCl_3$

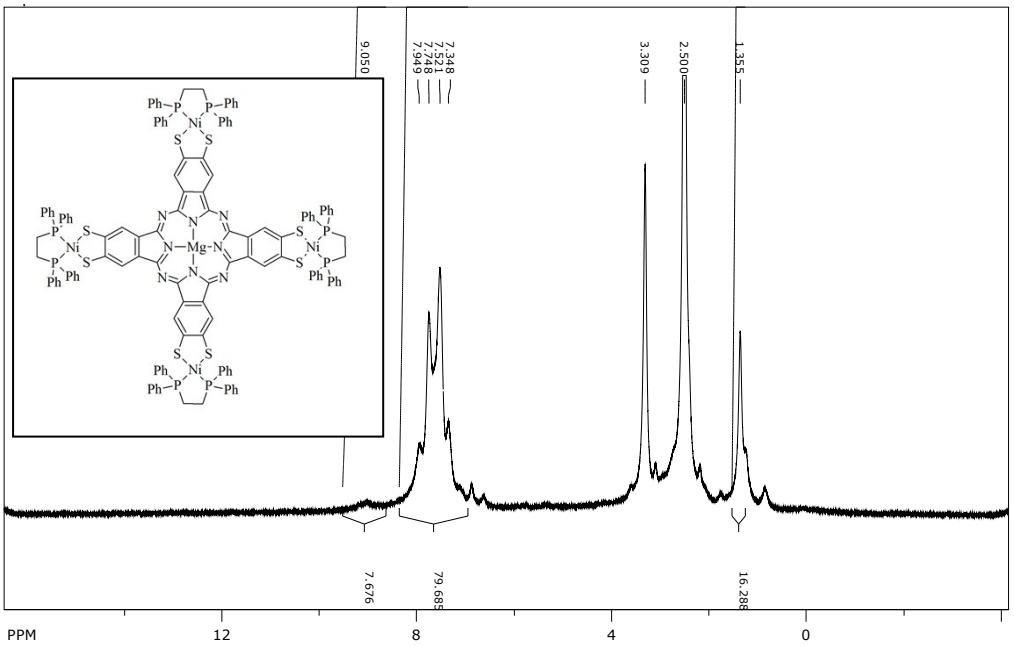

Figure S10. ^{1}H NMR of [(dppeNi)$_4$(S_8PcMg)] in DMSO-*d6*

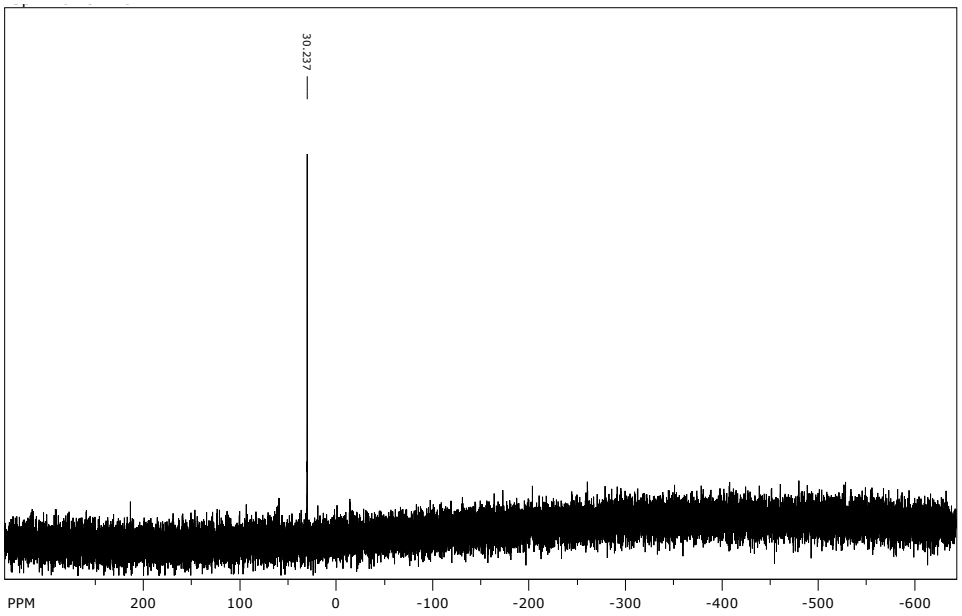

Figure S11. ^{31}P NMR of [(dppeNi)$_4$(S_8PcMg)] in DMSO-*d6*

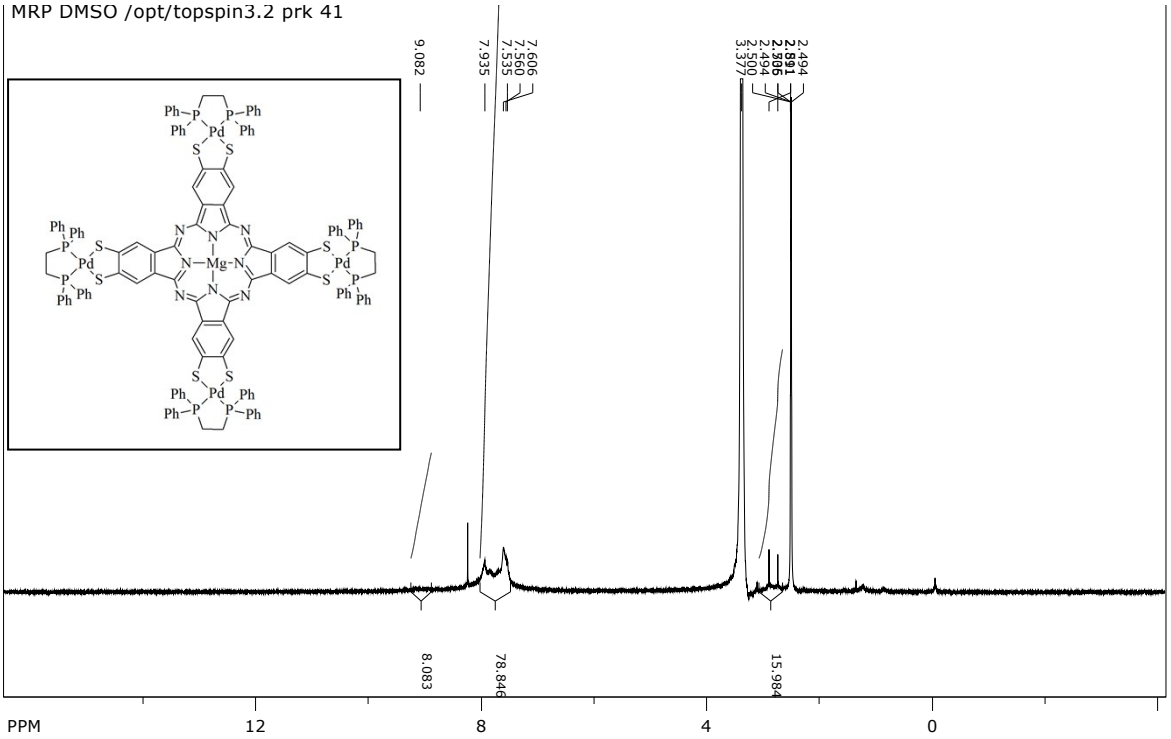

Figure S12. ^{1}H NMR of [(dppePd)$_4$(S_8PcMg)] in DMSO-*d6*

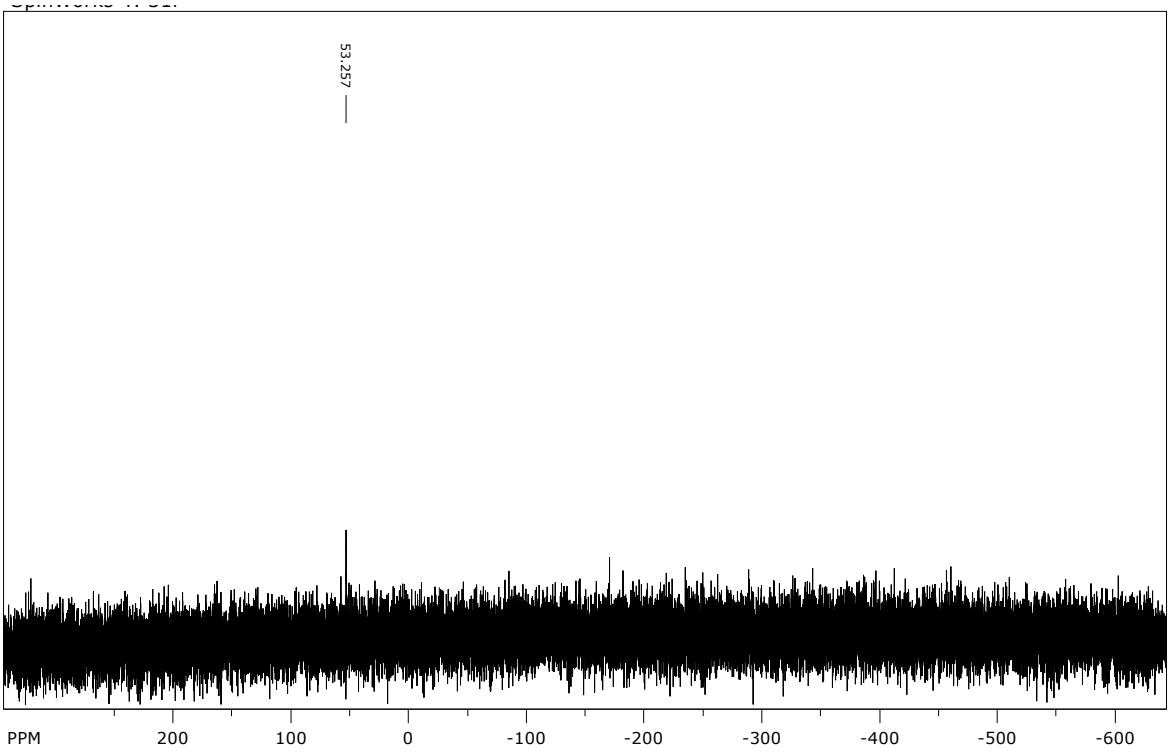

Figure S13. ^{31}P NMR of [(dppePd)$_4$(S_8PcMg)] in DMSO-*d6*

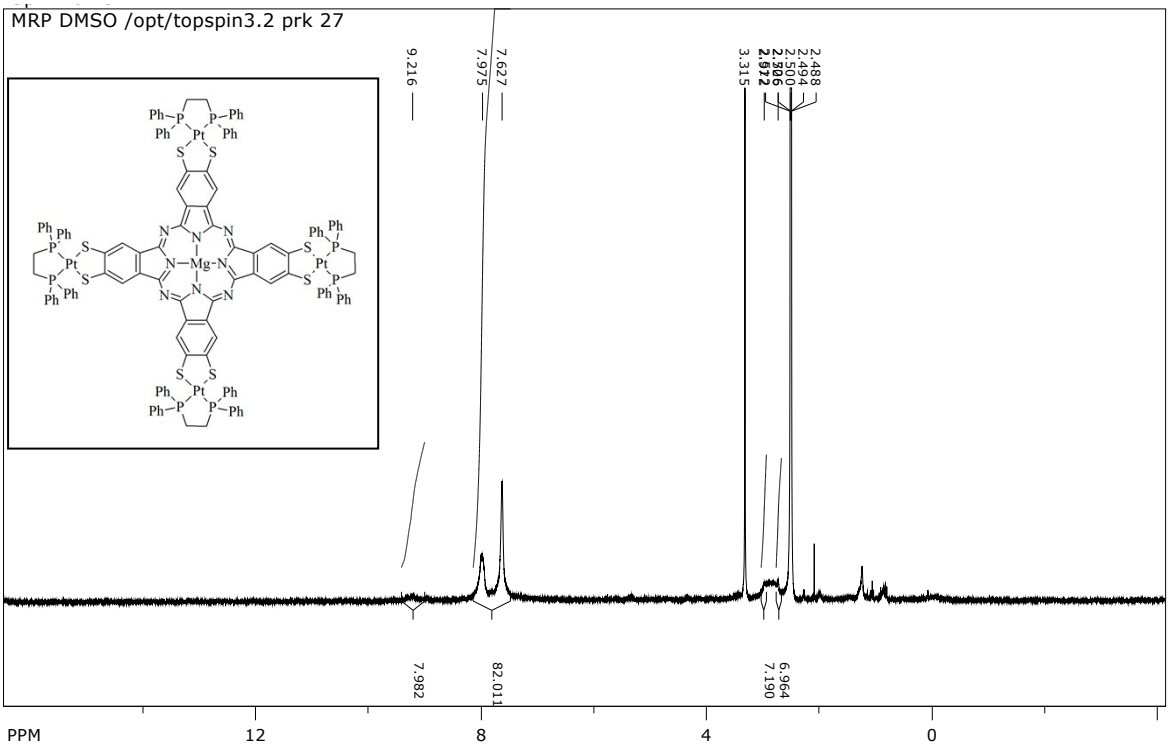

Figure S14. ^{1}H NMR of [(dppePt)$_4$(S$_8$PcMg)] in DMSO-*d6*

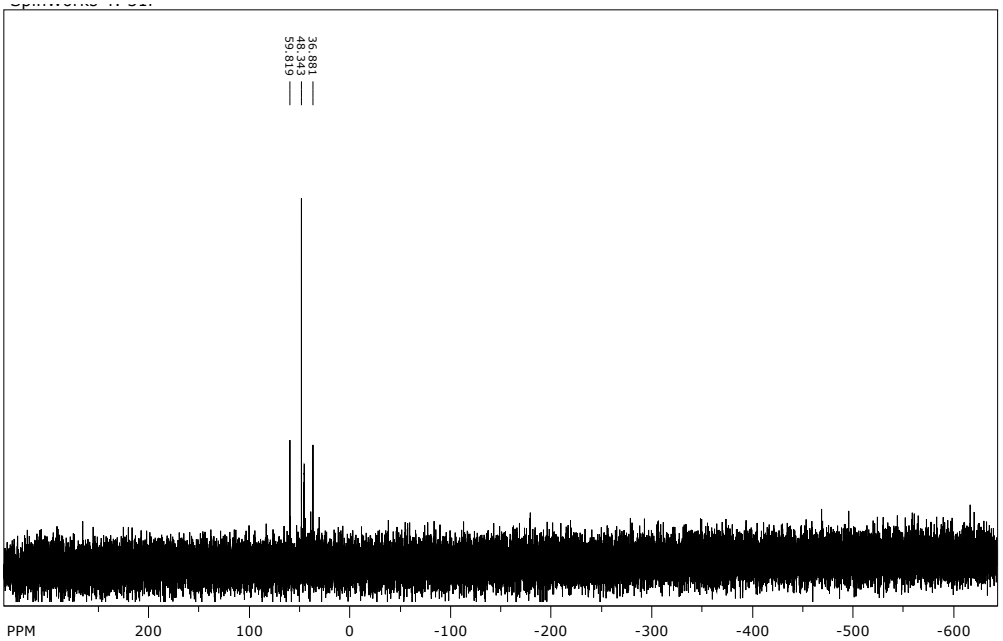

Figure S15. ^{31}P NMR of [(dppePt)$_4$(S$_8$PcMg)] in DMSO-*d6*

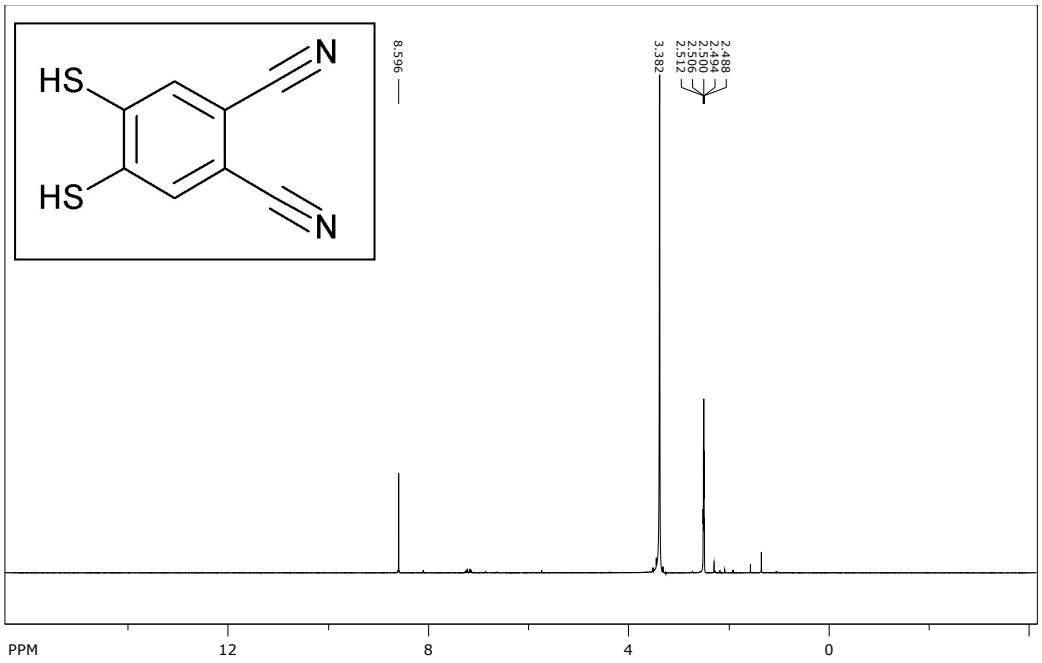

Figure S16. ^{1}H NMR of H_2dtpn in DMSO-*d6*

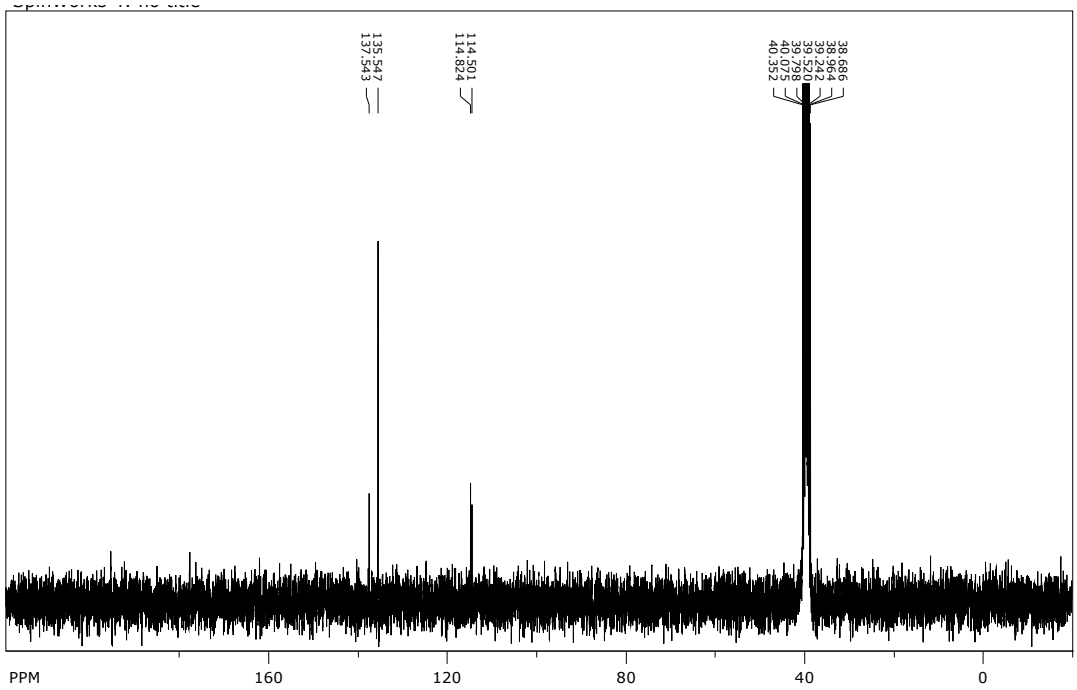

Figure S17. ^{13}C NMR of H_2dtpn in DMSO-*d6*

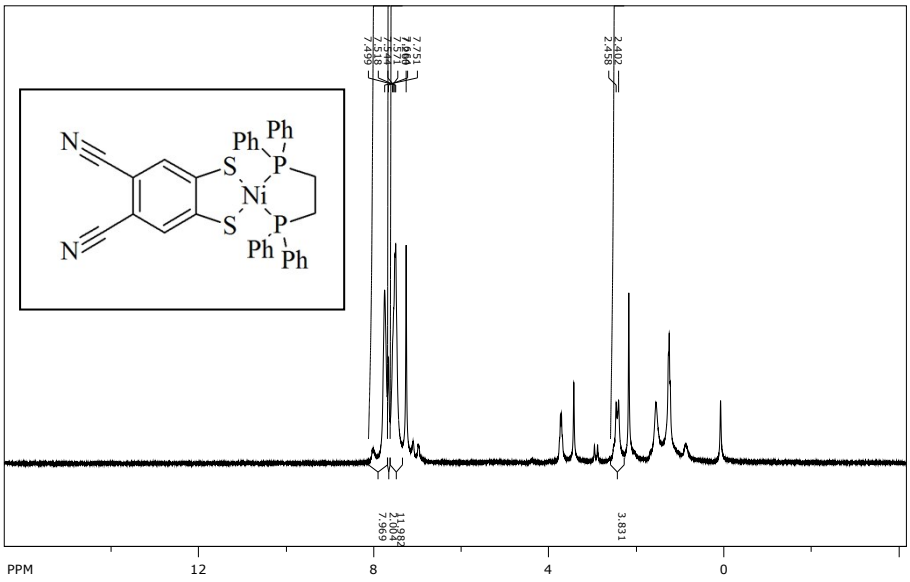

Figure S18. ^{1}H NMR of [Ni(dtpn)(dppe)] in $CDCl_3$

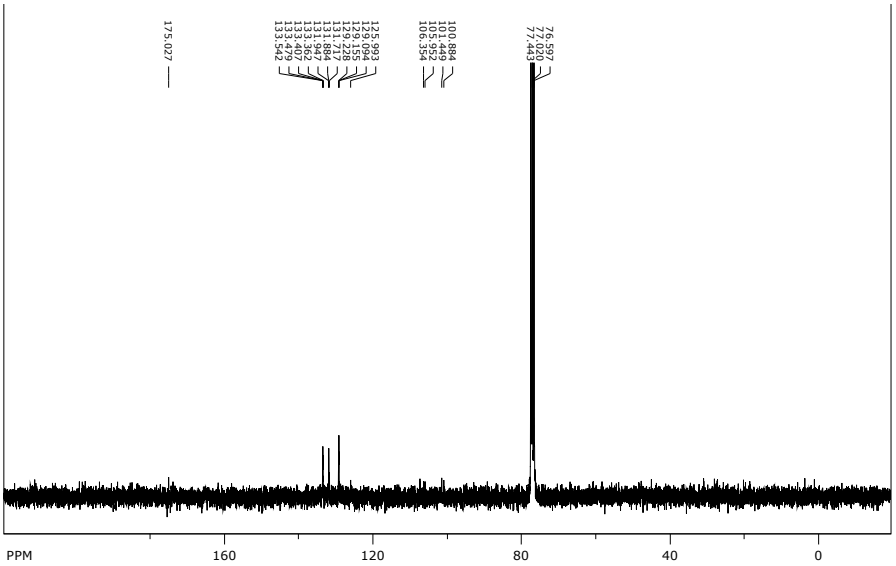

Figure S19. ^{13}C NMR of [Ni(dtpn)(dppe)] in $CDCl_3$

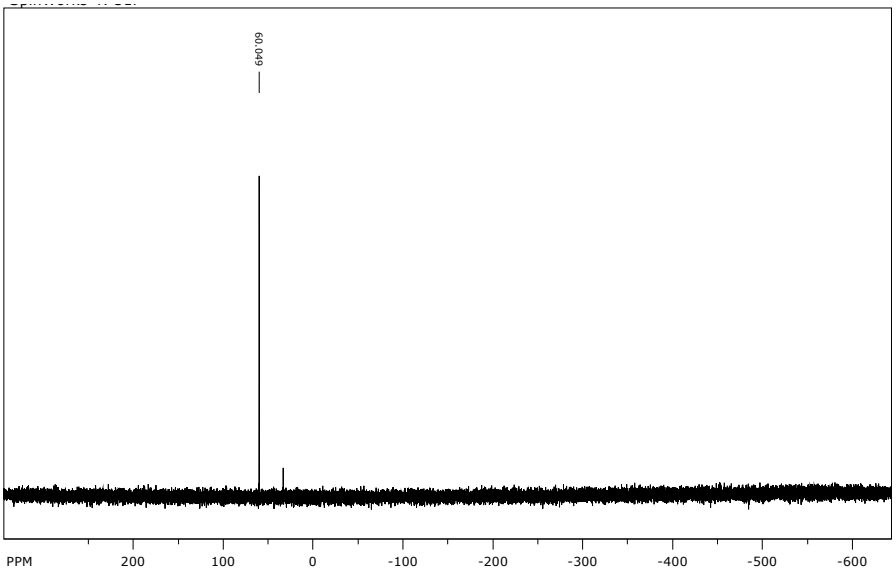

Figure S20. ^{31}P NMR of [Ni(dtpn)(dppe)] in $CDCl_3$

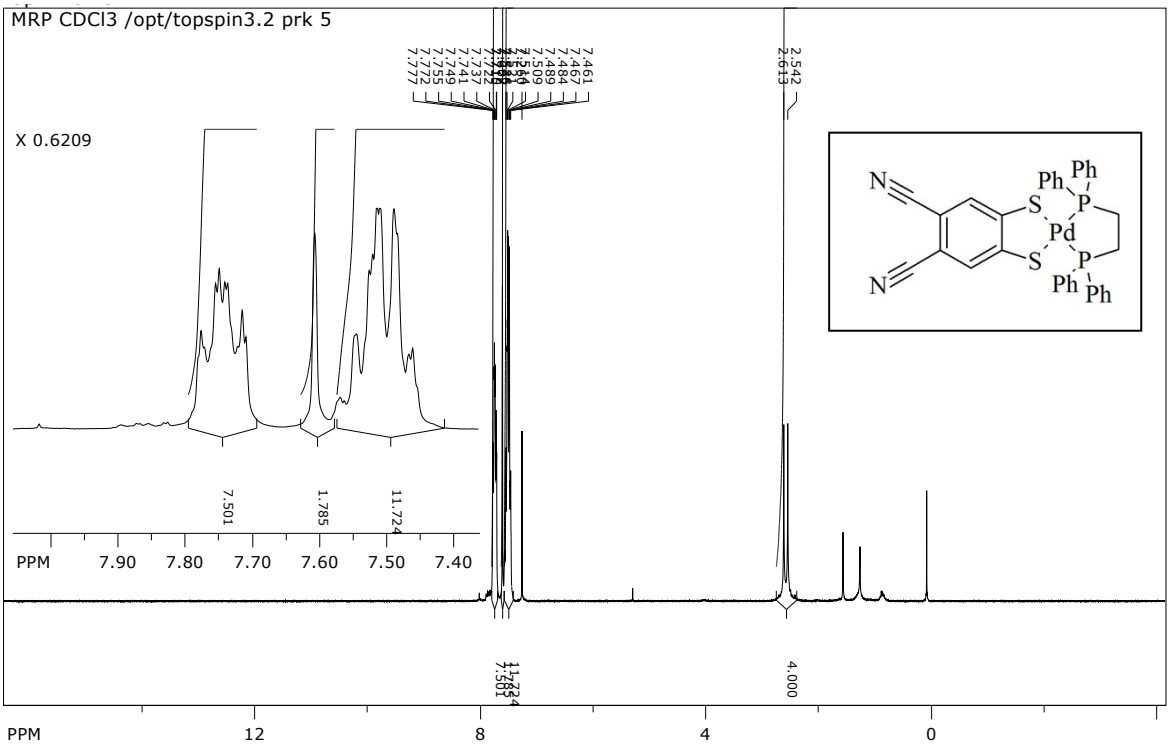

Figure S21. ^{1}H NMR of [Pd(dtpn)(dppe)] in $CDCl_3$

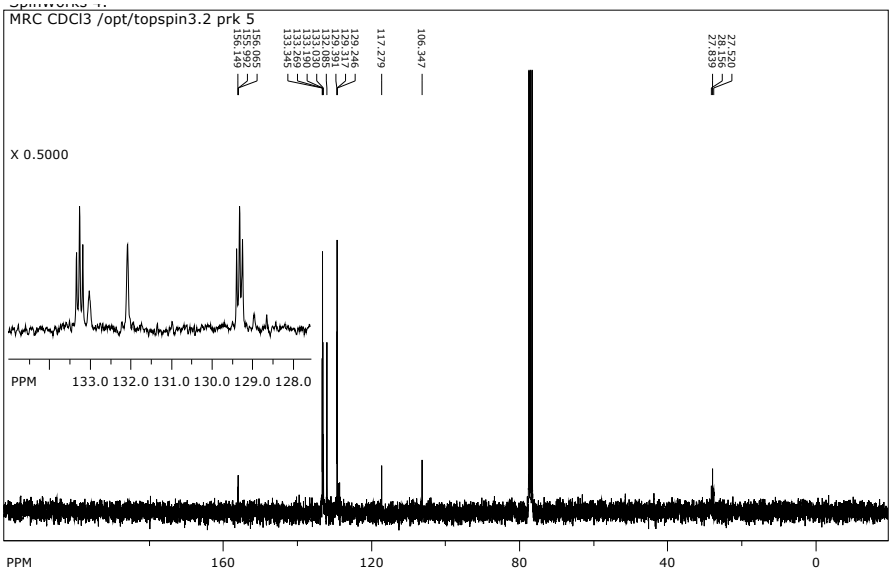

Figure S22. ^{13}C NMR of [Pd(dtpn)(dppe)] in $CDCl_3$

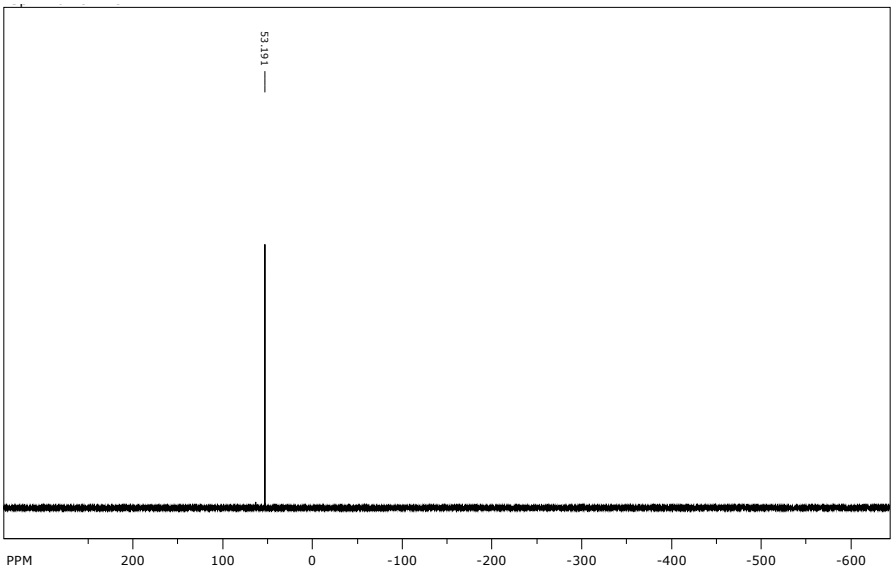

Figure S23. ^{31}P NMR of [Pd(dtpn)(dppe)] in $CDCl_3$

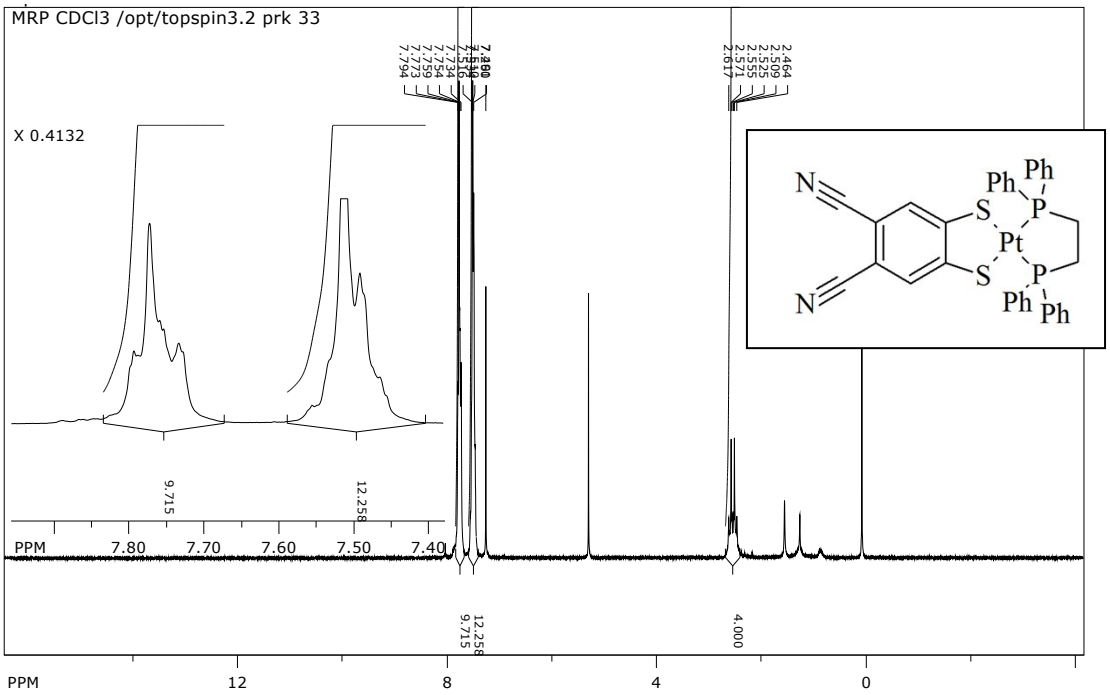

Figure S24. ^{1}H NMR of [Pt(dtpn)(dppe)] in $CDCl_3$

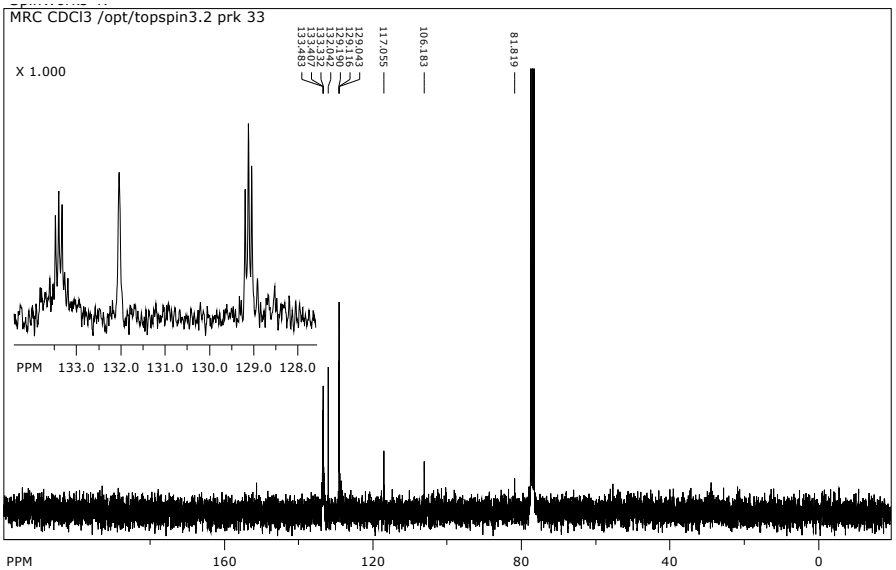

Figure S25. ^{13}C NMR of [Pt(dtpn)(dppe)] in $CDCl_3$

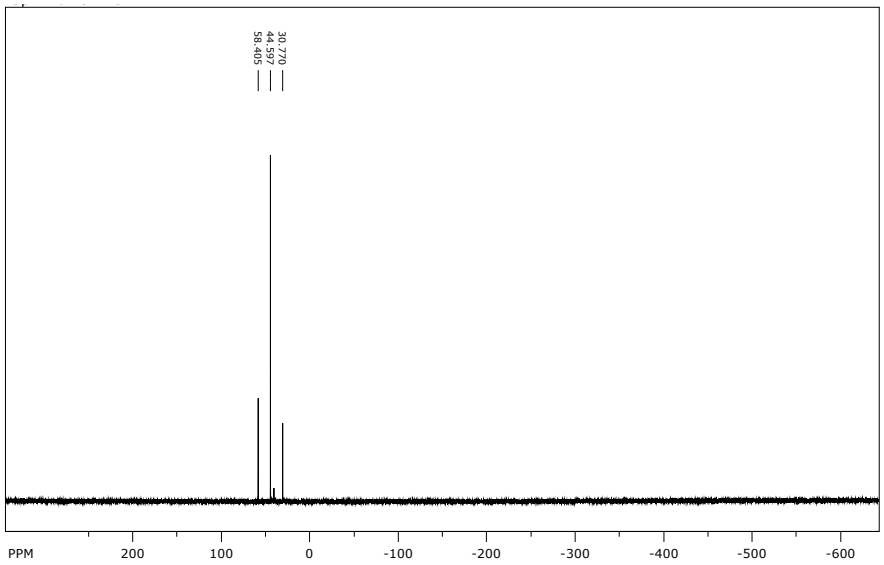

Figure S26. ^{31}P NMR of [Pt(dtpn)(dppe)] in $CDCl_3$

Mass Spectrometry

2,5-Dihydroxybenzoic acid (DHB) was used as matrix forMALDI-TOF meassurtements.

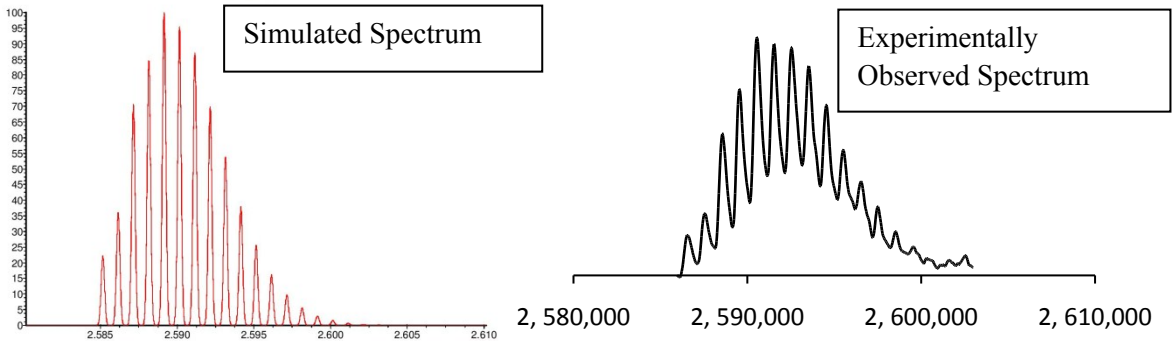

Figure S27: Simulated (left) and obtained (right) MALDI-TOF MS spectra for $[(dppeNi)_4(S_8PcMg)]$

$[(dppeNi)_4(S_8PcMg)]$ appears to readily fragment during the ionization process of MALDI-TOF MS. Several fragments could be identified, that related in general to the loss of a $[Ni(dppe)]^{2+}$ moiety.

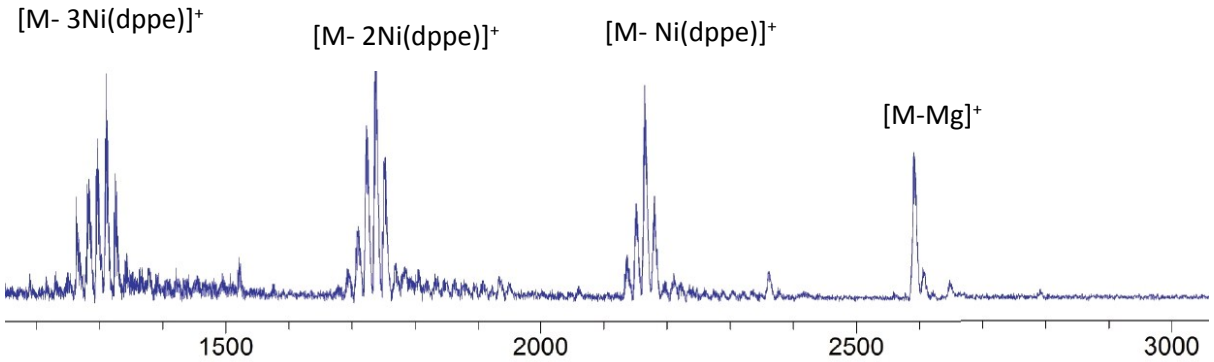

Figure S28: MALDI-TOF spectrum for $[(dppeNi)_4S_8PcMg]$. Not only the parent molecular ion, but also fragments formed by loss of $[Ni(dppe)]^{2+}$ can be identified.

For [[(dppePd)$_4$S$_8$PcMg], ionization only caused the loss of the Mg ion, but not the fragmentation of the diphosphinopalladium ions. This complex was also less readily ionized than the previously shown Ni complex, presumably due to the larger molecular weight. For [(dppePt)$_4$S$_8$PcMg], no complex could be seen by MALDI-TOF MS. We assume that the large molecular weight and favourable π-π stacking as well as metal interactions prevent this complex from being volatilized while still intact.

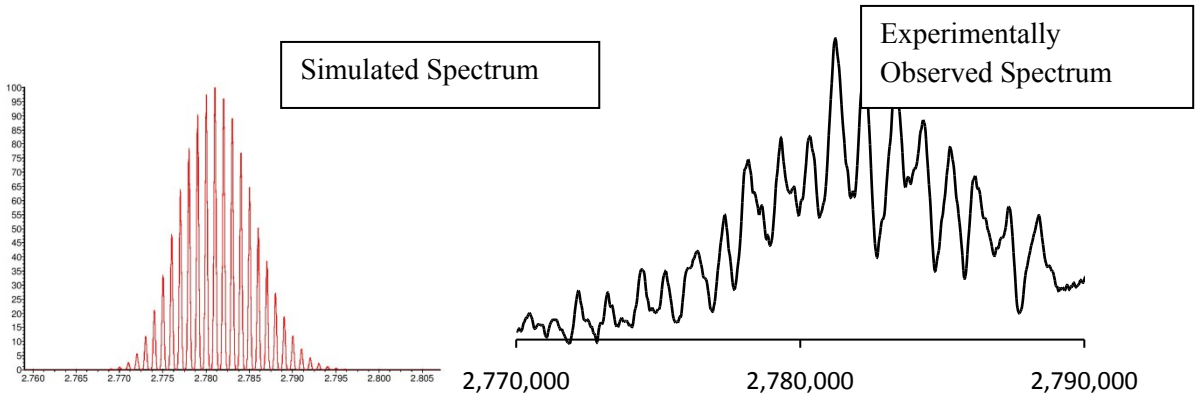

Figure S29: Simulated (left) and obtained (right) HR MALDI-TOF spectra for [(dppePd)$_4$S$_8$PcMg].

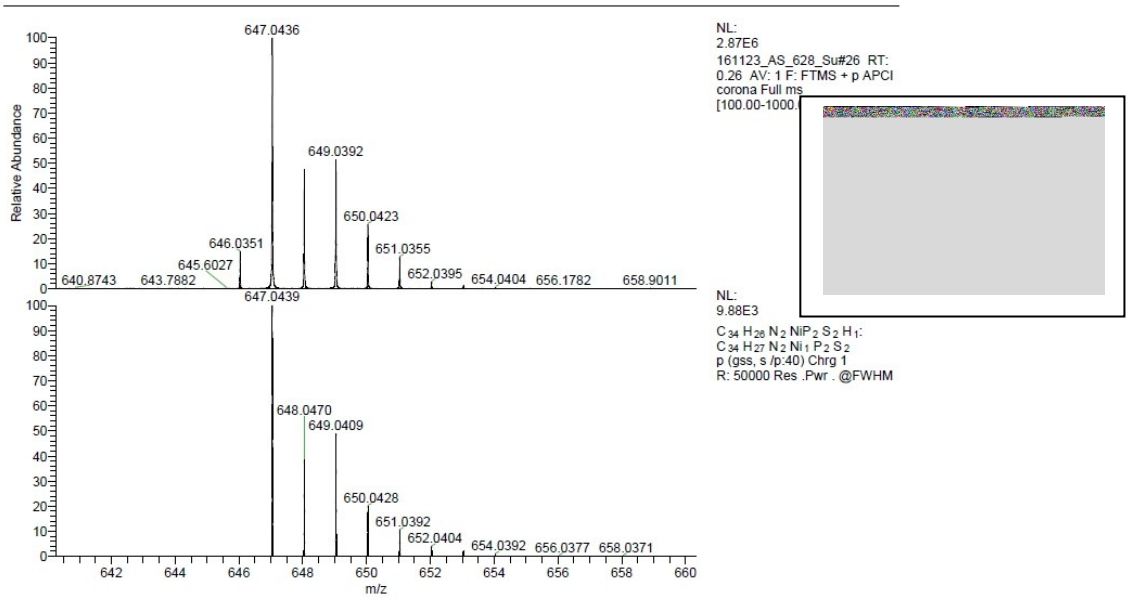

Figure S30: Simulated and obtained HRMS APCI+ spectra for [Ni(dtpn)(dppe)]

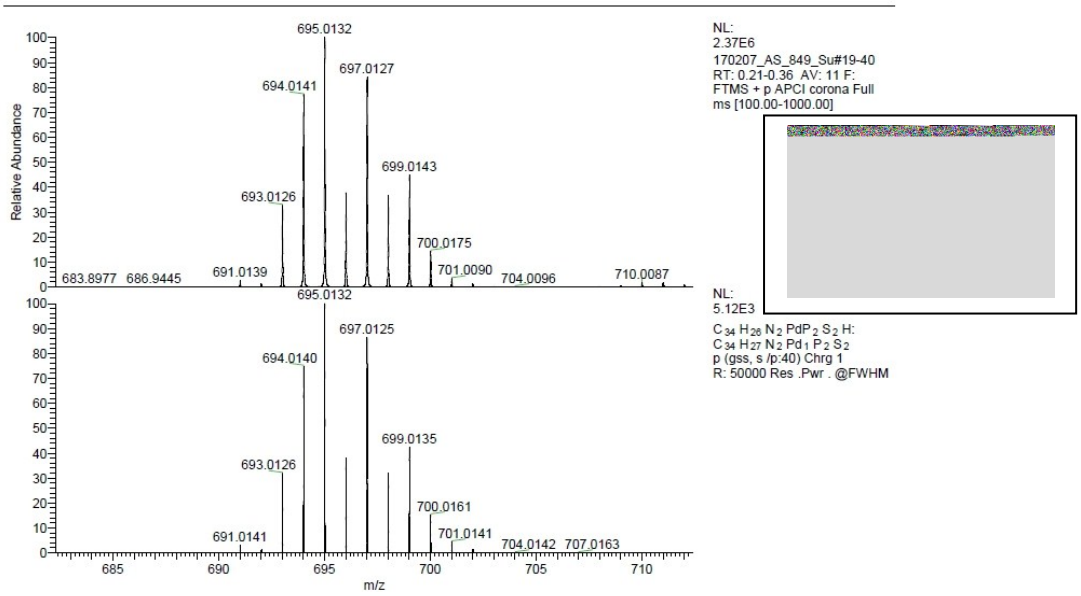

Figure S31: Simulated and obtained HRMS APCI+ spectra for [Pd(dtpn)(dppe)]

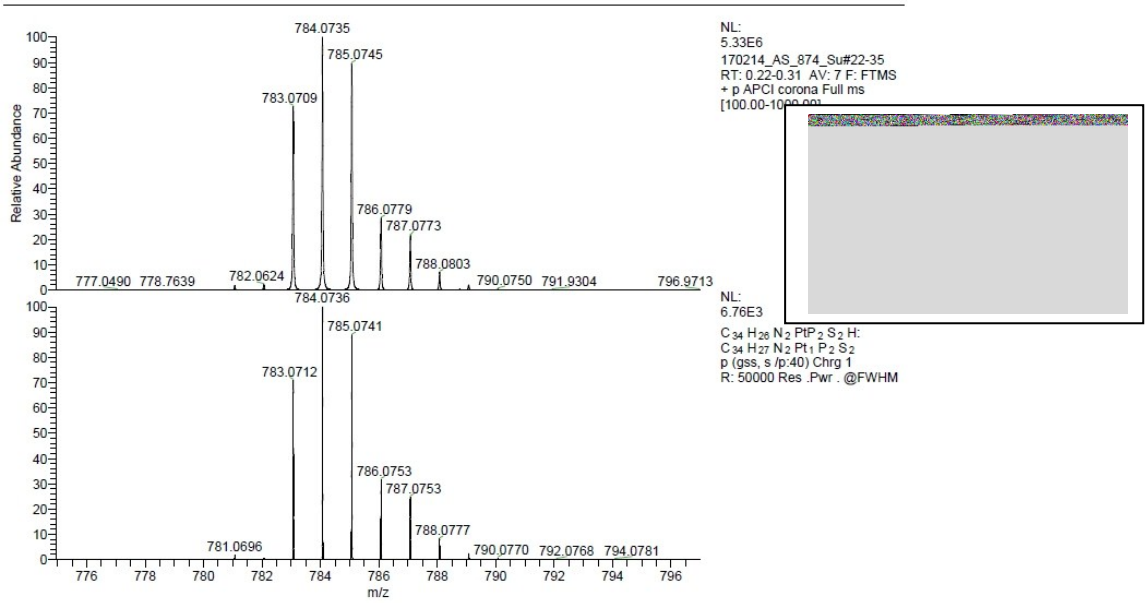

Figure S32: Simulated and obtained HRMS APCI+ spectra for [Pt(dtpn)(dppe)]

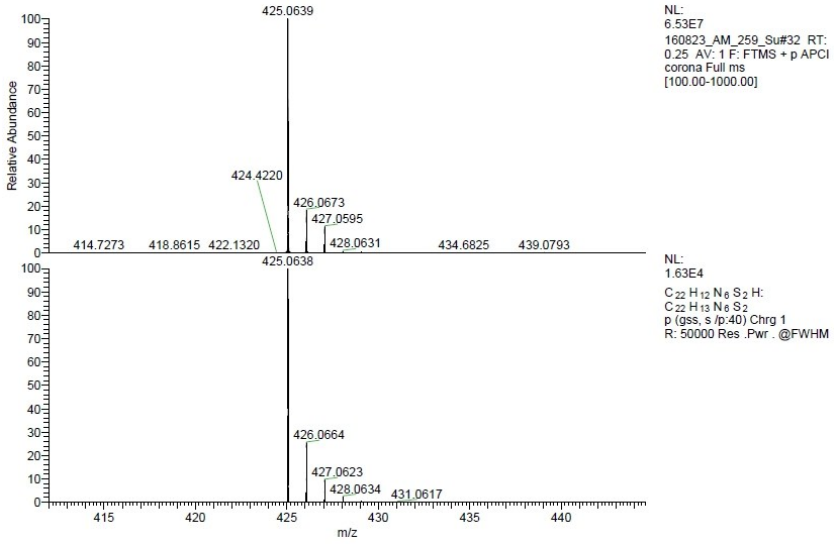

Figure S33: Simulated and obtained HRMS APCI+ spectra for the dinitrile precursor dbtpn

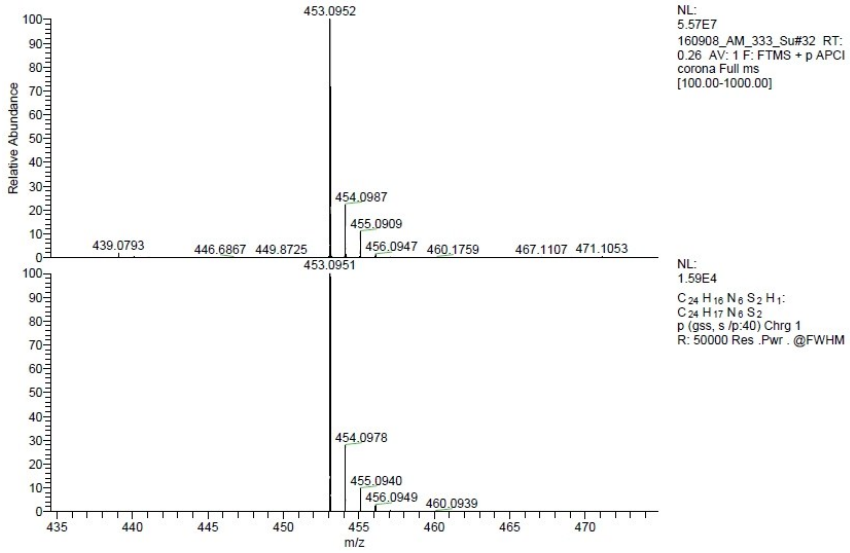

Figure S34: Simulated and obtained HRMS APCI+ spectra for the dinitrile precursor dmbtpn

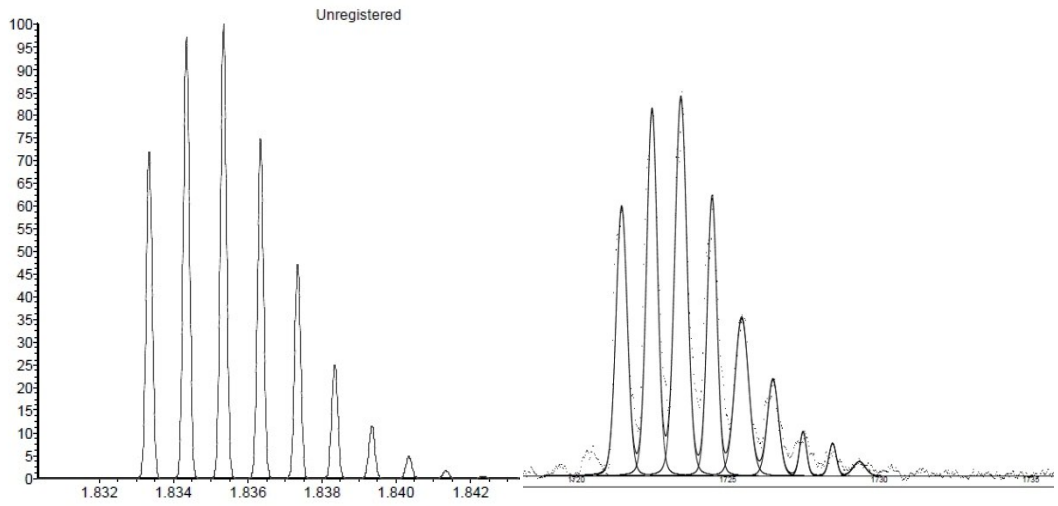

Figure S35: Simulated (left) and experimentally obtained (right) MALDI-TOF spectra for [$(RS)_8$PcMg]

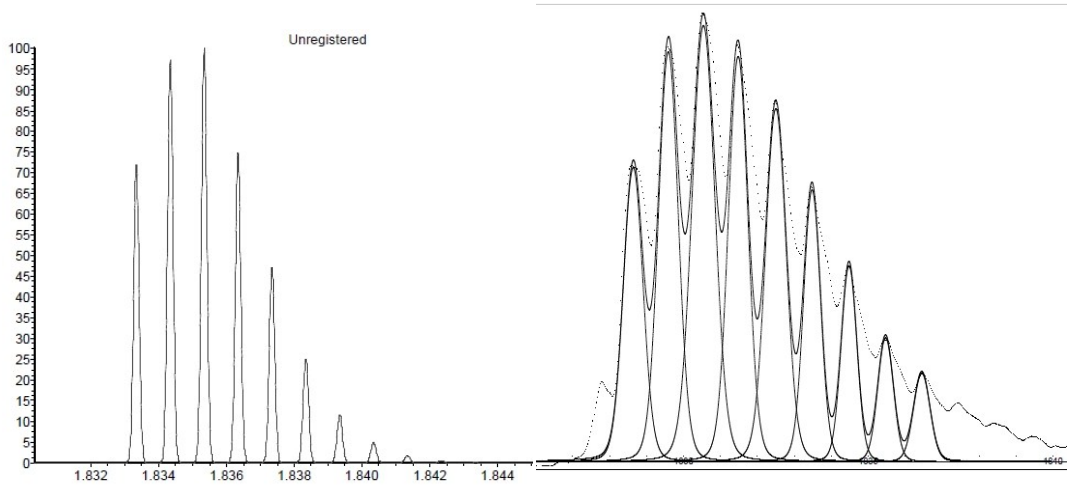

Figure S36: Simulated (left) and experimentally obtained (right) MALDI-TOF spectra for [(^{Me}RS)$_8$PcMg]

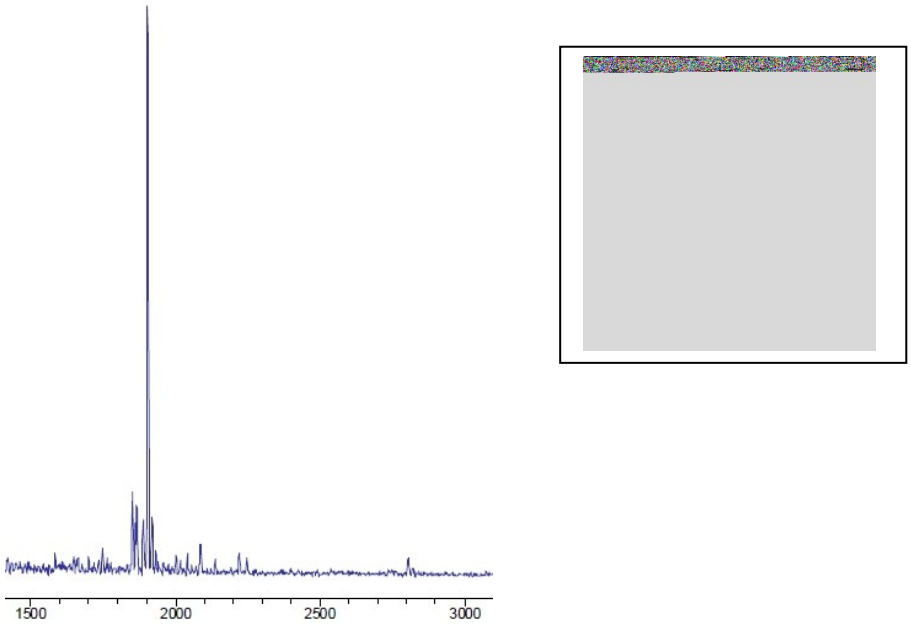

Figure S37. MALDI-TOF MS for [(Me$_3$Sn)$_8$S$_8$PcMg] (Monoisotopic mass = 1906.7). Ionisation of the complex resulted in a loss of one SSnMe$_3$ fragment. No parent molecular ion peak was seen, as shown here. Resolution in the spectrum is too poor to determine the isotopic pattern.